JOURNAL OF GEOPHYSICAL RESEARCH, VOL. 105, NO. A6, PAGES 13,103–13,117, JUNE 1, 2000

Plasma sounding at the upper hybrid frequency

M. E. Dieckmann,[1] S. C. Chapman,[2] A. Ynnerman,[1]
and G. Rowlands[2]

Abstract. A sounder measures the density of plasmas in various parts of the solar system. The sounder emits wave pulses into the ambient plasma and listens to the response. Intensity peaks in the wave response are typically related to two mechanisms. One is provided by waves that are reflected off plasma inhomogeneities and propagate back to the emitting antenna, where they are then detected. The second is provided by waves propagating with the same group velocity as that of the receiving antenna. In the second case the waves stay close to the antenna and thus yield a long-lasting response. Response peaks to sounding at the upper hybrid (UH) frequency have, in most cases, been related to reflected waves. In this work we examine if accompanying waves can give rise to the UH response peak. We examine quantitatively how the plasma response to sounding at the UH frequency depends on the plasma density, on the electron temperature, and on the emission amplitude. For the first two parameters this is done by solving the linear dispersion relation. The well-known property of the UH waves to change from having a zero group velocity to propagating waves, depending on how the electron density compares to the electron cyclotron frequency, is applied to Alouette sounder data. It is discussed how the change in the group velocity may affect the spectral profile of the UH resonance. We present results from numerical particle in cell (PIC) simulations which show that in the case of nonpropagating UH waves, energy can be coupled into the plasma even though the vanishing group velocity of the UH waves should not allow this. The PIC simulations and sounder data from the Alouette mission show that in the case of propagating UH waves the response duration to sounding may be used to determine the electron temperature. Emission amplitudes that are typical for plasma sounders are also shown to suppress the generation of certain electron cyclotron harmonic waves.

1. Introduction

A plasma sounder measures the plasma densities in parts of the solar system [*Décréau et al.*, 1993; *Etcheto et al.*, 1981; *Fejer and Calvert*, 1964]. The sounder emits a wave pulse into the ambient plasma and listens to the response. The peaks of the wave response at certain frequencies are commonly explained by two mechanisms. One mechanism is the excitation of waves with a group velocity close to the spacecraft velocity in the plasma frame of reference. Such waves are called accompanying waves. For sounding frequencies close to these frequencies the wave energy will remain close to the satellite. The plasma response sampled by the receiving antenna is then strong and long-lasting. The second mechanism explains the resonances by the excitation of oblique echoes [*McAfee*, 1969]. Waves with frequencies close to resonance frequencies are reflected back onto the receiving antenna by plasma inhomogeneities.

Resonances that are commonly attributed to oblique echoes are the plasma frequency ω_p, the harmonics of the electron cyclotron frequency ω_c, and the upper hybrid (UH) frequency $\omega_{uh} = \sqrt{(\omega_p{}^2 + \omega_c{}^2)}$ [*Benson*, 1977; *Le Sager et al.*, 1998]. The resonances at the frequency maxima (the f_q) of the electron cyclotron harmonic (ECH) waves with frequencies above ω_{uh} are attributed to accompanying waves [*Warren and Hagg*, 1968; *Benson*, 1977; *Le Sager et al.*, 1998]. This separation is, however, not strict. In the work of *Fejer and Calvert* [1964], accompanying waves have been named as a possible reason for the response at ω_{uh}.

In this work we investigate the emission of UH waves by means of particle in cell (PIC) simulations and by comparing the simulation results with the results predicted by the solution of the linear dispersion relation. The aim is to see if accompanying waves could be a mechanism for the plasma response peak at ω_{uh}. A sim-

[1]Inst. foer Teknik och Naturvetenskap, University of Linkoeping, Norrkoeping, Sweden.
[2]Physics Department, University of Warwick, Coventry, England, United Kingdom.

Paper number 1999JA900491.
0148-0227/00/1999JA900491$09.00

ple antenna model is implemented as the wave source. The linear dispersion relation for ECH waves propagating perpendicular to the magnetic field $\vec{B}$ with frequencies close to ω_{uh} is solved. The group velocities are calculated, and the response time to sounding at ω_{uh} is estimated assuming that accompanying waves are the reason for the plasma response. We assume that the most long-lasting plasma response at ω_{uh} is given by a plane ECH wave with its wave vector parallel to the antenna axis. The antenna axis is aligned perpendicular to $\vec{B}$. We assume that the spacecraft velocity in the plasma frame of reference is zero. Then the longest lasting response is given by the ECH wave with the lowest group velocity. We estimate the response time by dividing the antenna length by the group velocity of the slowest wave. This is clearly an oversimplified model for the real (three-dimensional) sounding experiment, but its only purpose is to give us an estimate for the response time. This estimate agrees with the response time provided by the PIC simulations. It is also in reasonable agreement with the response times measured by the Alouette mission.

In section 2 we revise how the plasma response to sounding at ω_{uh} changes with the ratio ω_p/ω_c and with a changing electron temperature. For $\omega_p/\omega_c < 1.7$ ($\omega_{uh}/\omega_c < 2$) the UH waves have a zero group velocity. In the opposite case they are propagating waves [*Akhiezer et al.*, 1975]. A change in the plasma response duration at $\omega_p/\omega_c = 1.7$ has been reported by *Fejer and Calvert* [1964]. In the work of *McAfee* [1969] the change in the topology of the ECH wave solutions close to ω_{uh} (and thus indirectly the group velocity) has been used to derive the conditions for oblique echoes at ω_{uh} which predicted correctly qualitative features of the UH response to sounding. The change in the group velocity has, to the knowledge of the authors, not previously been applied in the context of accompanying UH waves, and we examine this here.

It is shown that for increasing electron temperatures the wave group velocity strongly increases. This increase may be the reason for the absence of a plasma response to sounding at ω_{uh} in the hot parts of the magnetotail [*Etcheto et al.*, 1981] and in the Io plasma torus [*Le Sager et al.*, 1998]. The absence of these resonances may, however, also be related to a decreasing antenna response function for increasing wavelengths [*Meyer-Vernet et al.*, 1993].

Nonzero electron temperatures are shown to change the frequency at which the plasma response to sounding peaks. This change is, however, small, so that it should not have any impact on the sounding experiment. The response peak is shifted below ω_{uh} for $\omega_p/\omega_c < 1.7$ (strongly magnetized plasma). It is shifted above ω_{uh} in the opposite case (weakly magnetized plasma). It is also shown that for the plasma parameters under consideration the UH response in a strongly magnetized plasma should be relatively narrow banded in frequency whereas it should be relatively wide banded in the case of a weakly magnetized plasma. Up to this point the waves are assumed to be linear; that is, they are solutions of the linear dispersion relation.

In principle, it is possible to examine the generation of a wave packet by a pulse using the saddle point method described by *Brillouin* [1960]. Waves close to ω_{uh} have an electrostatic and an electromagnetic wave component. It is thus not possible to approximate the linear dispersion relation either by the electrostatic limit or by the electromagnetic limit. In addition, we cannot assume a plasma sounder to generate linear waves due to the strong emission amplitudes (the emission amplitudes for the Cluster sounder are 50 or 200 V [*Décréau et al.*, 1993], which compares to temperatures of the magnetospheric cold electron population of 1 eV [*Etcheto et al.*, 1981]).

Instead, a one and a half dimensional electromagnetic PIC code is employed. It solves the nonlinear Vlasov equation together with the full set of the Maxwell equations. The equations are solved in one spatial dimension for all three velocity components. The emission is modeled by applying electrostatic fields that oscillate in time to a set of simulation grid cells. Section 3 describes in more detail the simulation code, the plasma parameters, and the antenna.

In section 4 the case of propagating UH waves is investigated, which requires the plasma to be weakly magnetized. Then the plasma supports two wave solutions at ω_{uh}. Simulations for two emission amplitudes are compared. It is shown that for the typically strong sounder emission amplitudes the wave solution with the high wavenumber cannot be excited. The strong emission amplitudes excite waves in a regime in which electron trapping nonlinearly damps electrostatic waves propagating perpendicular to $\vec{B}$ [*Riyopoulos*, 1986]. The observation from the simulations that the absorption mechanism is more efficient for the wave with the high wavenumber is also consistent with electron trapping being the relevant damping mechanism. Direct evidence that this is the nonlinear damping mechanism requires, however, a detailed investigation of the electron phase space distribution, which is left to future work.

The properties of the plasma response, sampled by a virtual antenna placed in the simulation box, are investigated. Of particular interest is the question of whether the antenna length and the signal duration could be used to determine the electron thermal velocity. It is shown that this is indeed possible for the simple case of a one-dimensional geometry and an antenna that is at rest with respect to the plasma frame of reference.

Section 5 deals with the case of sounding in a strongly magnetized plasma. Sounding at ω_{uh} generates a nonpropagating, localized standing wave. Simulations for two emission amplitudes are compared. They show that the plasma response power is quadratically dependent on the emission amplitude and that it is linearly dependent on the emission time. The energy transport

into the plasma required to build up the standing wave is achieved by wave forerunners described, for example, by *Brillouin* [1960]. The nonpropagating perturbation is consistent with the observation by *Fejer and Calvert,* [1964] that the signal response at ω_{uh} is long-lasting in the case of a strongly magnetized plasma. The results are then discussed in section 6.

2. Kinetic Theory

The focus in our study is on ECH waves propagating perpendicular to $\vec{B}$. These wave modes are linearly undamped. The dispersion relation has been derived using the tensor components D_{xx}, D_{yy}, D_{xy}, and D_{yx} in the notation of *Krall and Trivelpiece* [1986]. Since the dispersion relation close to ω_{uh} is examined, the electromagnetic components of the waves cannot be ignored. In what follows, v_{th} is the electron thermal velocity. The phase and the group velocities of the waves are referred to as v_{ph} and v_{gr}. The frequencies are normalized to ω_c; that is, $\tilde{\omega} = \omega/\omega_c$. The wavenumbers are normalized to the inverse electron thermal gyroradius; that is, $\tilde{k} = kv_{th}/\omega_c$.

2.1. The Dispersion Relation of a Weakly Magnetized Plasma

The solutions of the linear dispersion relation in a weakly magnetized plasma close to $\tilde{\omega}_{uh}$ and for $v_{th} = 9.4 \times 10^5$ m/s are shown in Figure 1. Plotted is $\tilde{\omega}$ versus $\tilde{k}$. The horizontal solid lines show the harmonics of ω_c. The dashed line shows $\tilde{\omega}_{uh} = \sqrt{\tilde{\omega}_p^2 + 1} = 2.1$. The dots are the $\tilde{\omega}$ values calculated by the linear dispersion relation solver. The dashed line intersects with the linear dispersion relation at points 1 and 2. Some properties of these points are examined in section 4. Point 3 in Figure 1 shows an f_q. These nonpropagating wave solutions provide an important class of resonances to sounding [*Warren and Hagg,* 1968]. Some properties of these waves have been investigated by means of PIC simulations by *Dieckmann et al.* [1999].

At low $\tilde{k}$ in Figure 1 we get the (electromagnetic) slow extraordinary mode (at low $\tilde{\omega}$) and fast extraordinary mode (at high $\tilde{\omega}$). For increasing $\tilde{k}$ the fast extraordinary mode approaches asymptotically the ordinary wave mode. For the slow extraordinary mode (in the cold plasma limit) we get the limits for $k \to \infty$: $\tilde{\omega} \to \tilde{\omega}_{uh}$ and $v_{gr} \to 0$. The same limits for $\tilde{\omega}, v_{gr}$ are approached by a purely electrostatic ECH wave in the branch containing ω_{uh} for $\tilde{k} \to 0$ (warm plasma). Figure 1 shows that both limits incorrectly describe the low $\tilde{k}$ waves with $\tilde{\omega} \approx \tilde{\omega}_{uh}$. The slow extraordinary mode goes over into the ECH wave branch containing $\tilde{\omega}_{uh}$ and $v_{gr} \neq 0$ at $\tilde{\omega} \approx \tilde{\omega}_{uh}$.

We focus on the UH waves at low $\tilde{k}$ as the accompanying waves providing the strong plasma response to sounding. In section 4 the numerical simulations will show why the UH waves at point 2 in Figure 1 can be ignored.

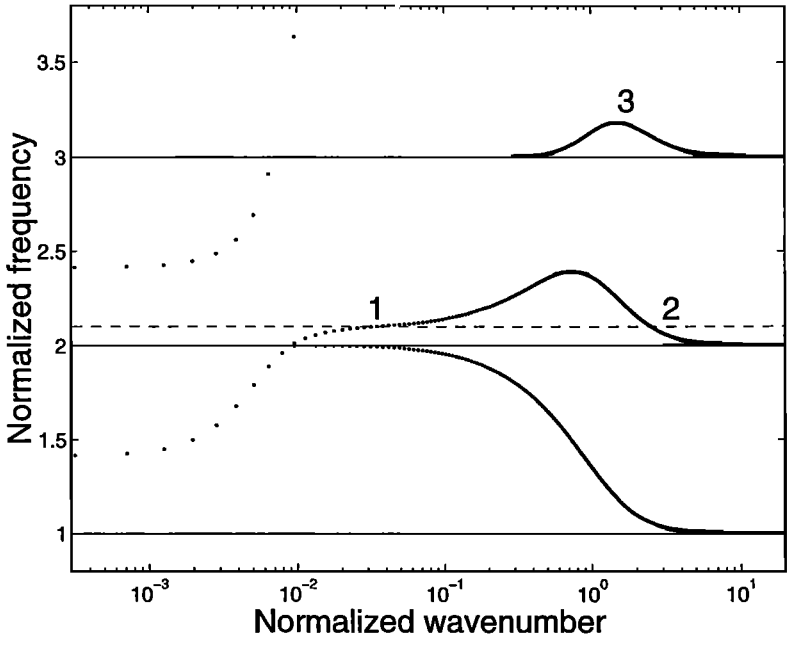

Figure 1. The solution of the linear dispersion relation for undamped electron cyclotron harmonic (ECH) waves and $\omega_p/\omega_c > 1.7$. Overplotted are the harmonics of ω_c (solid lines) and ω_{uh} (dashed line). Points 1 and 2 show the central $\tilde{\omega}, \tilde{k}$ of the wave modes excited in the simulations. Point 3 shows an f_Q which is another type of resonance to plasma sounding.

We calculate, for $\tilde{\omega}_{uh} = 2.1$, the v_{gr} of the resonance as a function of $\tilde{k}$ for three sample v_{th}. We then determine the minimum value of v_{gr} at $\tilde{\omega} \approx \tilde{\omega}_{uh}$ and its $\tilde{\omega}$. For $v_{th} = 10^5$ m/s we determine the minimum as $v_{gr} \approx 2.26 \times 10^4$ m/s at $\tilde{\omega}_{\min} = 2.101$. For $v_{th} = 5 \times 10^5$ m/s the values are $v_{gr} \approx 2.33 \times 10^5$ m/s and $\tilde{\omega}_{\min} = 2.106$. For $v_{th} = 10^6$ m/s the values are $v_{gr} \approx 5.92 \times 10^5$ m/s at $\tilde{\omega}_{\min} \approx 2.116$.

In the limit of low v_{th} we get $\tilde{\omega}_{\min} \to \tilde{\omega}_{uh}$ and $v_{gr} \to 0$ as we would expect. For increasing v_{th} both $\tilde{\omega}_{\min}$ and v_{gr} increase. For v_{th} larger than $v_{th} \approx 1.5 \times 10^6$ m/s the minimum in v_{gr} disappears. In this case the waves with $\tilde{\omega} \approx \tilde{\omega}_{uh}$ are dominated by the slow extraordinary mode which has a large v_{gr}. For sufficiently high v_{th} any wave energy injected into the plasma should propagate away quickly, thus giving a very short response to sounding. If a sounder does not sample the wave response immediately after the emission has finished, i.e., if it has a dead time [*Décréau et al.*, 1993; *Le Sager et al.*, 1998], the plasma response may be short enough to go undetected. This may be the reason for the absence of any plasma response at $\tilde{\omega}_{uh}$ in the hot parts of the magnetotail [*Etcheto et al.*, 1981] and in the Io plasma torus [*Le Sager et al.*, 1998].

As an illustration, we take parameters for the plasma and the spacecraft velocity encountered by the Ulysses sounder in the Io plasma torus [*Le Sager et al.*, 1998]. We set $\omega_p/\omega_c = 4.9$. For simplicity we take a single Maxwellian with a temperature of 10 eV for the electron distribution function. At $\tilde{\omega}_{uh} = 5.001$, $v_{gr} \approx 1.85 \times 10^5$ m/s. The lowest value $v_{gr} \approx 1.71 \times 10^5$ m/s close to ω_{uh} is found at $\tilde{\omega} = 5.007$.

We assume the antenna axis to be parallel to the spacecraft velocity vector in the plasma frame of reference. The antenna axis orientation is also assumed to be perpendicular to $\vec{B}$, and we assume that the strongest plasma response comes from ECH waves propagating perpendicularly to $\vec{B}$. The emission generates wave packets propagating away from the antenna. The antenna measures the potential difference between the antenna wires. The wave electric fields of the emitted wave packet can only contribute to the plasma response if the wave packet's end did not leave the space between the end points of the antenna wires. This will be shown in section 4.3 to be true for a one-dimensional antenna at rest with respect to the plasma frame of reference.

According to *Le Sager et al.* [1998], the antenna frame of reference moves in the Io plasma torus with $\approx 10^5$ m/s relative to the ambient plasma. The UH waves have, for the parameters above, a $v_{ph} \approx 5.8 \times 10^7$ m/s, and thus the Doppler shift is negligible. The wave packet that leaves the space between the antenna's end points last is the wave propagating in the same direction as the spacecraft in the plasma frame of reference. Its propagation velocity is given by its v_{gr} minus the relative velocity of the spacecraft with respect to the plasma frame of reference. We obtain the plasma response duration seen at an antenna by dividing the antenna length by the wave packet's propagation velocity in the antenna frame of reference. For the UH wave the response duration for the Ulysses antenna with a length of 72 m should then be 0.85 ms. The maximum response duration for waves close to ω_{uh} should be 1 ms. The Ulysses receiver starts to sample the wave response 5 ms [*Le Sager et al.*, 1998] after the emission has finished. No wave response due to accompanying UH waves can thus be expected.

In section 4 the emission of a wave packet with $\tilde{\omega} = \tilde{\omega}_{uh}$ is investigated by means of PIC simulations. The emission should excite wave solutions at the intersection points 1 and 2 in Figure 1 of $\tilde{\omega} = \tilde{\omega}_{uh}$ with the linear dispersion relation solution of the corresponding ECH branch. Both waves have the same $\tilde{\omega}$ but different $\tilde{k}$, implying different thresholds for the electric field value required to trap electrons. This field threshold has been derived by *Riyopoulos* [1986]. According to equation (3) in the work of *Riyopoulos* [1986], trapped particle islands emerge in a plasma if the normalized amplitude $A_i = (eE_0kn\sqrt{8})/[m{\omega_c}^2 r_i\sqrt{(\pi r_i)}]$ of a monochromatic ECH wave exceeds the normalized frequency departure $\delta = \omega/\omega_c - n$ from a harmonic of ω_c. Here E_0 is the electric field amplitude of the wave, n is the cyclotron harmonic number, e/m is the electrons' characteristic charge to mass ratio, and r_i is the normalized velocity vk/ω_c of the ith trapped particle island center. We set $A_i = \delta$, and we replace ω and k by $\tilde{\omega}$ and $\tilde{k}$. Then the expression for the critical electric field in V/m is

$$E_{\text{crit}} = \frac{1}{2}(\tilde{\omega} - n)\frac{m}{e}\frac{r_i v_{th}\omega_c}{n\tilde{k}}\left(\frac{\pi r_i}{2}\right)^{1/2}. \qquad (1)$$

Equation (1) determines the electric field value required to trap electrons. A wave electric field exceeding this threshold has been shown to nonlinearly damp the wave [*Riyopoulos*, 1986]. It has been derived for a monochromatic wave with $\omega \approx n\omega_c$. Both these assumptions are not necessarily fulfilled in our case, but (1) nevertheless indicates that the wave mode at high $\tilde{k}$ should be saturated at much weaker field amplitudes than the wave mode at a low $\tilde{k}$. In section 4.1, numerical simulations show that an emission with a strong electric field amplitude can only generate the ECH wave with the low $\tilde{k}$. This observation would be consistent with the prediction of (1) that the high $\tilde{k}$ wave is suppressed by trapping.

2.2. The Dispersion Relation of a Strongly Magnetized Plasma

The linear dispersion relation solution for a strongly magnetized plasma and for frequencies close to $\tilde{\omega}_{uh}$ is shown in Figure 2. Here $\tilde{\omega}$ is plotted versus $\tilde{k}$. The dots indicate the $\tilde{\omega}$ values calculated by the linear dispersion relation solver. The vertical solid lines show the harmonics of ω_c. The dashed line shows $\tilde{\omega}_{uh} = 1.9$. At low $\tilde{k}$ we identify the slow extraordinary mode at low $\tilde{\omega}$ and the fast extraordinary mode at high $\tilde{\omega}$. The s-

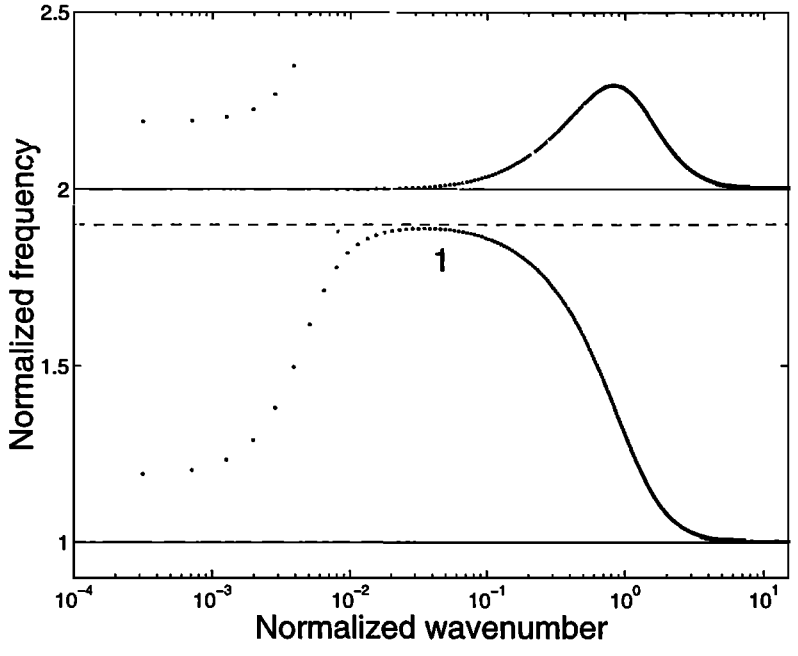

Figure 2. The solution of the linear dispersion relation for undamped ECH waves and $\omega_p/\omega_c < 1.7$. Overplotted are the harmonics of ω_c (solid lines) and ω_{uh} (dashed line). Point 1 indicates the $\tilde{\omega}, \tilde{k}$ excited in the simulations.

low extraordinary mode goes over into the ECH branch containing $\tilde{\omega}_{uh}$. In section 5 we will discuss the emission of a wave packet with $\tilde{\omega} = \tilde{\omega}_{uh}$. A wave should be excited at the intersection point between $\tilde{\omega}_{uh}$ and the lowest ECH branch (indicated by point 1). The minimum of $|v_{gr}|$ at $\tilde{\omega} \approx \tilde{\omega}_{uh}$ is always zero like for point 3 in Figure 1. Contrary to the latter resonance, however, point 1 in Figure 2 depends on v_{th}. The resonant wave has an $\tilde{\omega} \approx 1.899$ for $v_{th} = 10^5$ m/s, an $\tilde{\omega} \approx 1.894$ for $v_{th} = 5 \times 10^5$ m/s, and an $\tilde{\omega} \approx 1.888$ for $v_{th} = 10^6$ m/s. The change in $\tilde{\omega}$ is small for this interval of v_{th}.

2.3. Comparing the Width of the Response Peaks

In Figure 3 we plot $v_{gr}(\tilde{\omega})/v_{th}$ for $\tilde{\omega}_{uh} = 1.9$ (Figure 3a) and for $\tilde{\omega}_{uh} = 2.1$ (Figure 3b). The circles correspond to $v_{th} = 9.4 \times 10^5$ m/s, and the crosses correspond to $v_{th} = 10^5$ m/s. While the circles correspond to magnetospheric v_{th} [*Roennmark and Christiansen*, 1981] used for the numerical simulations in sections 4 and 5, the crosses are representative for the Earth's ionospheric v_{th} [*Baumjohann and Treumann*, 1997].

Figure 3a shows that $\tilde{\omega}_{uh}$ is not a plasma eigenmode. The gap between the ECH wave's maximum $\tilde{\omega}$ and $\tilde{\omega}_{uh}$ increases for increasing v_{th}. Figure 3a also shows that the v_{gr} are low for $\tilde{\omega} \approx \tilde{\omega}_{uh}$ only.

Figure 3b shows that the $\tilde{\omega}$ at which the ECH waves reach their minimum v_{gr} is above $\tilde{\omega}_{uh}$ and that it increases for increasing v_{th}. While for ionospheric v_{th} the minimum in v_{gr} is pronounced, it practically disappeared for magnetospheric v_{th}. Only for $\omega_p/\omega_c < 1.7$ and for $\tilde{\omega} \approx \tilde{\omega}_{uh}$ can we get $|v_{gr}| = 0$.

If the resonance at $\tilde{\omega}_{uh}$ is due to accompanying waves, the response time to sounding should reflect this. If we assume that the plasma response time for accompanying waves seen by an antenna at rest with respect to the plasma is approximately the antenna length divided by v_{gr}, we can relate the response time to v_{gr}.

In the work of *Fejer and Calvert* [1964] the observed response time to sounding at $\tilde{\omega}_{uh}$ is $\approx 10^4$ wave cycles for $\tilde{\omega}_{uh} < 2$ and 3×10^3 wave cycles for $\tilde{\omega}_{uh} > 2$. For a typical value in the ionosphere of $\omega_{uh} \approx 1.5 \times 10^6$ rad/s [*Fejer and Calvert*, 1964] the response durations are 6.7 and 2 ms, respectively (obtained by multiplying the response time in wave cycles by the wave period in physical units).

For an antenna length of the Alouette sounder of 45.7 m [*Benson et al.*, 1997], the observed response duration of 2 ms, and $v_{th} = 10^5$ m/s, we must have $v_{gr}/v_{th} = 0.23$. This is the value of the minimum v_{gr} in Figure 3b. Defining the width of the response peak as the frequency interval for which $|v_{gr}| < 0.46$ (half the response time of 2 ms) gives a spectral width of $0.014\ \omega_c$.

For a response duration of 6.7 ms, v_{gr}/v_{th} must be 0.068. This low value is only achieved for $\tilde{\omega}$ close to $\tilde{\omega}_{uh}$ (Figure 3a). Defining the spectral width of the response peak as the ω- interval for which $|v_{gr}| < 0.136$ (half the response time of 6.7 ms) gives a spectral width of $4 \times 10^{-4} \omega_c$. The spectral line for $\tilde{\omega}_{uh} < 2$ is thus narrow compared with the spectral line for the case $\tilde{\omega}_{uh} > 2$.

Finally, for a magnetospheric $v_{th} = 9.4 \times 10^5$ m/s and for $\tilde{\omega}_{uh} > 2$, the minimum v_{gr}/v_{th} is 0.58. The interval for which $|v_{gr}| < 1.16$ is $0.22\ \omega_c$. The maximum response duration for an antenna with a length of 45.7

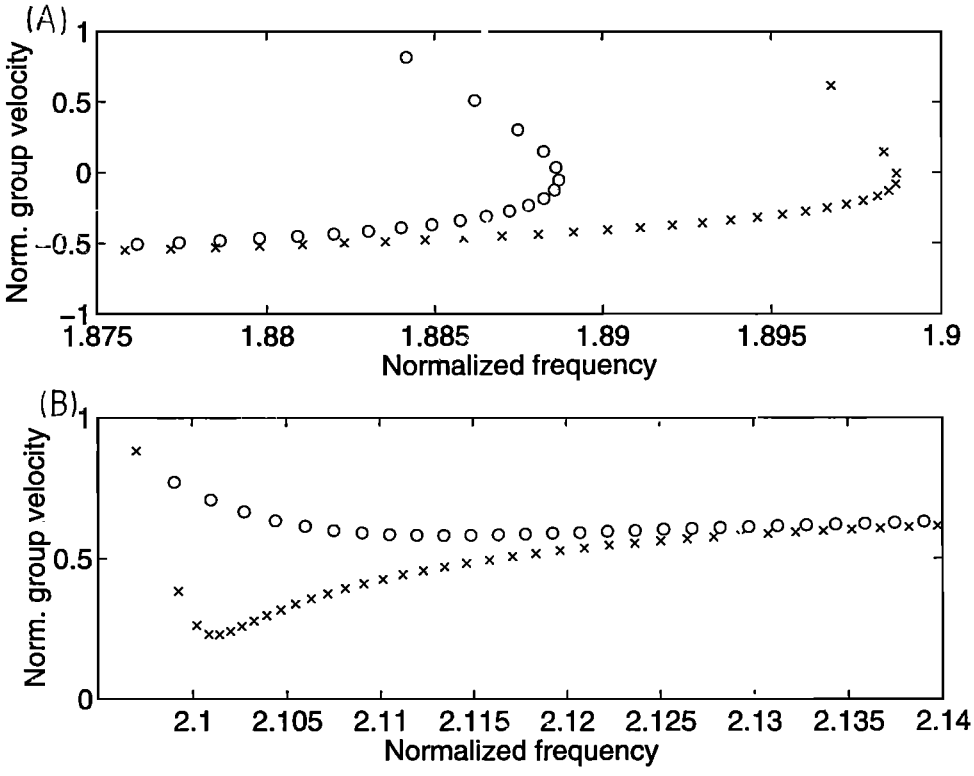

Figure 3. The dependence of v_{gr}/v_{th} on $\tilde{\omega}$ of the ECH waves. (a) $\omega_p/\omega_c < 1.7$. (b) $\omega_p/\omega_c > 1.7$.

m would be ≈ 0.08 ms. Thus the response would be broad in $\tilde{\omega}$ and of a short duration.

3. The Code and the Antenna

The emission of waves with $\tilde{\omega} = \tilde{\omega}_{uh}$ is investigated in sections 4 and 5 by means of PIC simulations. The electromagnetic and relativistic simulation code solves for one spatial and three velocity components of the particles and for the three vector components of the electric and the magnetic field. The simulation direction is in the x- direction. The external $\vec{B}$ is in the z- direction. The temperature for the electrons and the protons is 5 eV ($v_{th} \approx 9.4 \times 10^5$ m/s). The single Maxwellian electron and proton distributions are represented by 1024 particles per cell each. We set $\omega_p \approx 18.5$ kHz and vary ω_c to model the cases of a strongly magnetized plasma and a weakly magnetized plasma. The simulation box consists of 1500 grid cells, and each cell is $\Delta x = 7$ m long.

A typical emitting antenna on board a sounder consists of a pair of wires that is connected to a transmitter [*Décréau et al.*, 1993]. The exact current distribution on the antenna is not known during the emission process. In the numerical simulations we thus employ a simplified model for the antenna. We assume that the antenna can be represented by oscillating charge densities at one or two points in space. Since the numerical simulations model only one spatial dimension, the antenna corresponds to one or two plates with an infinite extention perpendicular to the simulation direction. Thus no electric fields other than those in the simulation direction are directly generated. In an unmagnetized plasma such waves would correspond to electrostatic waves. In a magnetized plasma, however, this separation is not apparent [*Krall and Trivelpiece*, 1986]. As discussed in section 2, the emitted wave at $\tilde{\omega}_{uh}$ at low $\tilde{k}$ is expected to have an electromagnetic component.

We assume that the potential difference is shielded over one Debye length, which is approximately one simulation grid cell. The antenna electric fields are nonzero only at one grid cell to each side of the antenna and have an opposite sign on these two cells. The electric fields at the grid cell m and $m+1$ are updated every (discrete) simulation time step $s\Delta t$ by adding an increment ΔE to the self-consistent electric field calculated by the PIC simulation. The self-consistent magnetic field calculated by the PIC simulation is not modified. The value for m is 750 in the case of an emission involving one emission plate. The two values for m are 745 and 755 for the emission involving two antenna plates. A schematic diagram showing the antenna electric fields (excluding the plasma response) as arrows is shown in Figure 4. The direction corresponds to the sign of the electric field, and the length corresponds to its absolute value. Figure 4a shows the one-plate emission, and Figures 4b and 4c correspond to the two-plate emission.

The increment ΔE is proportional to $\cos(\omega_0 s\Delta t)$. The emission frequency ω_0 is set to ω_{uh}. The total electric field then oscillates like $\sin(\omega_0 s\Delta t)$ in time (the

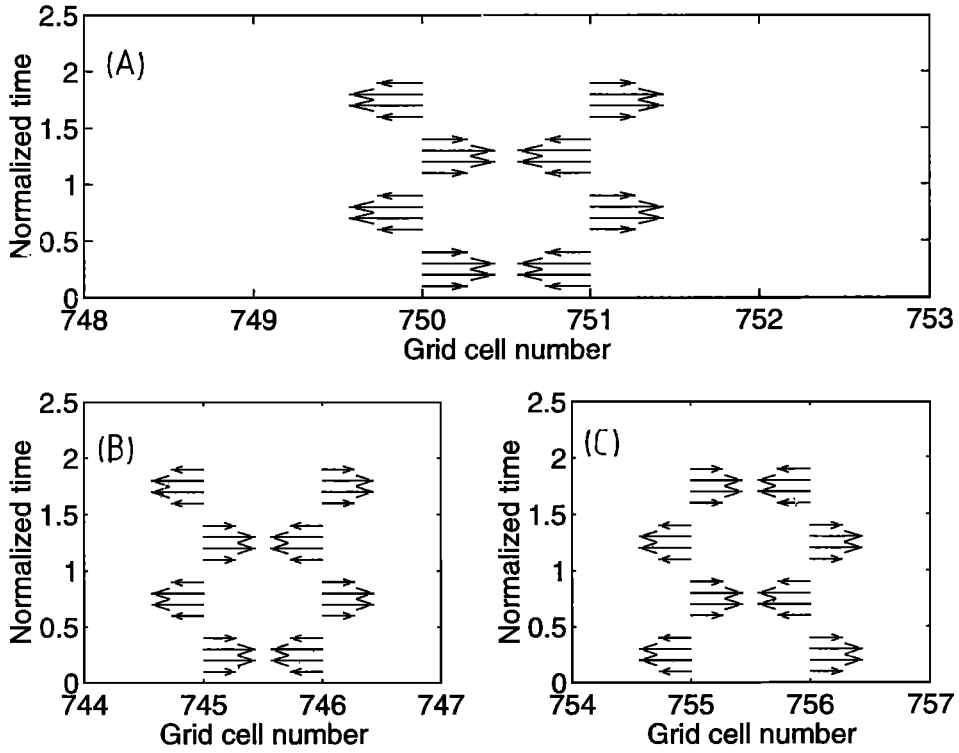

Figure 4. A schematic picture of the simulation antenna. (a) The electric fields as arrows for the emission with one sounder plate at the simulation cells 750 and 751. (b) The electric fields at the cells 745 and 746 (plate 1) for the emission with two plates. (c) The electric fields at the cells 755 and 756 (plate 2) for the emission with two plates.

summation in time of the ΔE is equivalent to an integration). The magnitude of ΔE is chosen such as to give the desired antenna electric fields (the relation between the increment and the resulting field oscillations is nontrivial owing to the electric fields generated by the plasma response to the antenna electric fields).

The antenna is assumed to be permeable for the particles; that is, no boundary conditions for the particles have been implemented at the antenna cells. Both the permeable antenna and the electric field distribution are unrealistic in that the antenna electric fields decrease linearly in the simulation owing to the field representation by linear splines. Debye shielding gives an exponentially decreasing potential. Since the generated waves have wavelengths that are long compared to the two antenna grid cells, we may ignore any effects introduced by the oversimplified antenna model.

In what follows, the physical times t_r will be normalized to $t = t_r/(2\pi/\omega_0)$. The value for ω_0 and thus the normalization change depending on if the plasma is strongly or weakly magnetized. The normalized emission duration is $T = 40$. For the considered ω_c this corresponds to $t_r \approx 2$ ms, which is twice as long as the emission duration of the Cluster or the Ulysses sounder [*Décréau et al.*, 1993; *Le Sager et al.*, 1998].

The antenna will couple predominantly to those ω, k for which the power spectrum of the antenna function $A(x,t_r)$ is large. Here $A(x,t_r)$ represents the spatial and temporal distribution of the electrostatic fields applied to the antenna grid cells. We employ two different antennas. One involves sinusoidally oscillating electric fields at the simulation grid cells 750 and 751 (one antenna plate case) and is employed in sections 4.1, 4.2, and 5. The second antenna involves the simulation grid cells 745, 746, 755, and 756 for the antenna with two plates (see Figure 4) and is used in section 4.3.

The electric fields (waves) arising from the plasma response are not included in $A(x,t_r)$. The power spectrum of $A(x,t_r)$ is given by $P(\omega, k)$. If, as a first approximation, the plasma response electric fields are ignored, $P(\omega, k)$ can be split up into a term depending on ω and a term depending on k.

For simplicity we calculate $P(\omega)$ by means of the Fourier integral. We refer to the unnormalized emission time as τ. The emission amplitude is zero outside $t_r \epsilon [0, \tau]$. For frequencies close to positive ω_0 it is sufficient to approximate $\sin(\omega_0 t_r)$ by $(1/2i)\exp(i\omega_0 t_r)$. Then the power spectrum is

$$P(\omega) = \frac{1}{4}\left|\int_0^\tau \exp(i\omega_0 t_r)\exp(-i\omega t_r)dt_r\right|^2 = \frac{\sin[(\omega_0-\omega)\tau/2]^2}{4(\omega_0-\omega)^2}. \quad (2)$$

Most wave power is concentrated in the interval $\omega \epsilon [\omega_0 - 2\pi/\tau, \omega_0 + 2\pi/\tau]$.

Our simulation box is periodic; that is, a minimum k exists. This is defined as $\Delta k = 2\pi/(M\Delta x)$, with M as the number of simulation grid cells and Δx as the length of each cell. We estimate $P(k)$ by means of a discrete Fourier transform:

$$P(k_l) = \left| 1/M \sum_{n=0}^{M-1} A_n \exp\left(-i2\pi k_l n/M\right) \right|^2 . \quad (3)$$

In physical units the wavenumber is $k = k_l \Delta k$. The time series A_n is, for the antenna with one plate, nonzero only at two grid cells. We set the values as $A_m = 1$ and $A_{m+1} = -1$; that is, the amplitudes at these cells have an opposite phase. Then the transform reduces to

$$P(k_l) = \left|\exp\left(-i2\pi k_l m/M\right)\left(1 - \exp\left(-i2\pi k_l/M\right)\right)\right|^2 = 4 \times \sin^2(2\pi k_l/(2M)) . \quad (4)$$

Note that k_l has an upper limit of $k_{Ny} = M/2$ (Nyquist theorem). This antenna thus couples most wave energy to high k and to $\omega \approx \omega_0$.

4. Simulated UH Emissions in a Weakly Magnetized Plasma

Let $\omega_c = 10$ kHz and $\tilde{\omega}_0 \equiv \tilde{\omega}_{uh} = 2.1$. At this emission frequency $\tilde{\omega}_0$ the (linear) plasma supports two waves with different $\tilde{k}$ (see Figure 1) and E_{crit}. According to *Riyopoulos* [1986], the ith trapped particle island's center is, for $r_i > 0.5n^2$, located at $r_i \approx i\pi + 0.5(n + 0.5)\pi$. The center of the zeroth trapped particle island (i=0) determines the electric field threshold for the onset of trapping. The emitted waves have $\tilde{\omega} \approx 2$. Thus the wave will first trap electrons at n=2 (n is the cyclotron harmonic number $n\omega_c$). We thus replace r_i in (1) by $r_0 \approx 3.9$. The intersection points of $\tilde{\omega} = 2.1$ and the linear dispersion relation have $\tilde{k}_1 = 0.035$ and $\tilde{k}_2 = 2.5$. The critical electric field for $\tilde{k}_1$ is $E_{\text{crit}} \approx 2.3$ V/m whereas it is $E_{\text{crit}} \approx 0.03$ V/m for $\tilde{k}_2$.

4.1. An Emission Amplitude of 1.2 V/m

The electric field amplitude for the virtual sounder is less than E_{crit} for $\tilde{k}_1 = 0.035$ but higher than E_{crit} for $\tilde{k}_2 = 2.5$. The peak potential difference $U_{\max}$ between the antenna plate and the plasma for $\Delta x = 7$ m is $U_{\max} = 8.4$ V, which is less than that for "real" sounders. For example, the sounder on board the forthcoming Cluster mission applies a $U_{\max}$ of either 50 or 200 V [*Décréau et al.*, 1993] between its antenna wires while the Ulysses sounder applies a $U_{\max}$ of 30 V.

The electrostatic field data provided by the simulation are Fourier-transformed over space. The Fourier transform is squared to give the power as a function of $\tilde{k}, t$. The power is integrated from $t = 40$ to $t = 80$. The result is shown in Figure 5. Plotted is the power, normalized to the peak power, as a function of $\tilde{k}$. Overplotted as dashed lines are the $\tilde{k}$ for which the linear dispersion relation solution intersects with $\tilde{\omega} = \tilde{\omega}_{uh}$. The wave power peaks at a $\tilde{k}$ close to the low $\tilde{k}$ intersection point. The maximum is, however, shifted toward higher values of $\tilde{k}$. The reason is discussed in section 4.2.

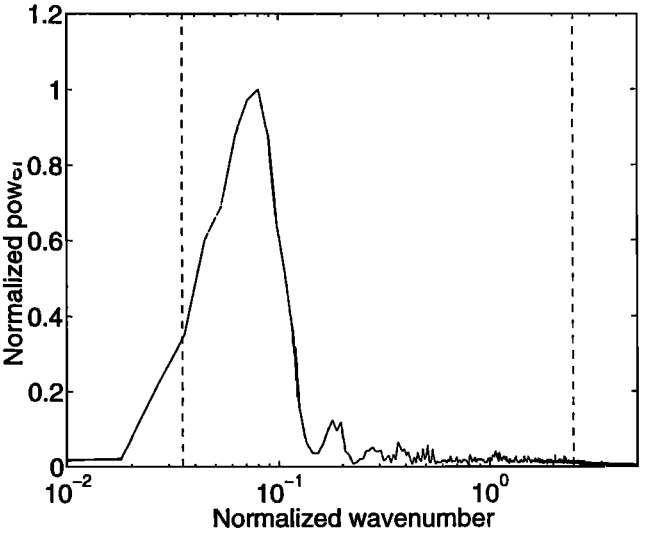

Figure 5. The normalized power of the wave modes as a function of $\tilde{k}$ for a strong emission and for $\omega_p/\omega_c > 1.7$. The power has been integrated over time. The dashed lines indicate the points where the solution of the linear dispersion relation crosses ω_{uh}.

In Figure 5 one also sees weak sidelobes of the main peak at $\tilde{k} \approx 9 \times 10^{-2}$. The maxima of these sidelobes are located at $\tilde{k} \approx 1.8 \times 10^{-1}$, $\tilde{k} \approx 2.7 \times 10^{-1}$, and $\tilde{k} \approx 3.6 \times 10^{-1}$. These sidelobes are harmonics of the peak at $\tilde{k} \approx 9 \times 10^{-2}$.

No wave power can be detected at the second intersection point at $\tilde{k} = 2.5$. The antenna power $P(k)$ derived in (4) predicts that this peak should have more power than the peak at $\tilde{k} = 0.035$. A nonlinear absorption mechanism must thus be present, absorbing the wave energy of the high $\tilde{k}$ mode.

4.2. An Emission Amplitude of 0.3 V/m

Now we apply $U_{\max} = 2.1$ V between the antenna plate and the surrounding plasma. The electrostatic field data are Fourier-transformed over space. The power spectrum as a function of $\tilde{k}, t$ is integrated over time. The integration is done over two integration subintervals, one from $t = 40$ to $t = 60$ and one from $t = 60$ to $t = 80$. Both subsets are normalized to half the peak power in Figure 5 to account for the shorter integration time. The power for the first subinterval is shown in Figure 6a. Plotted is the normalized power versus $\tilde{k}$. The dashed lines indicate the intersection points between the linear dispersion relation solution and $\tilde{\omega} = \tilde{\omega}_{uh}$. As in Figure 5, the peak at low $\tilde{k}$ is shifted toward higher $\tilde{k}$ than expected. The explanation is given below.

No sidelobes can be detected in this case. The self-interaction of the wave at low $\tilde{k}$ is negligible compared

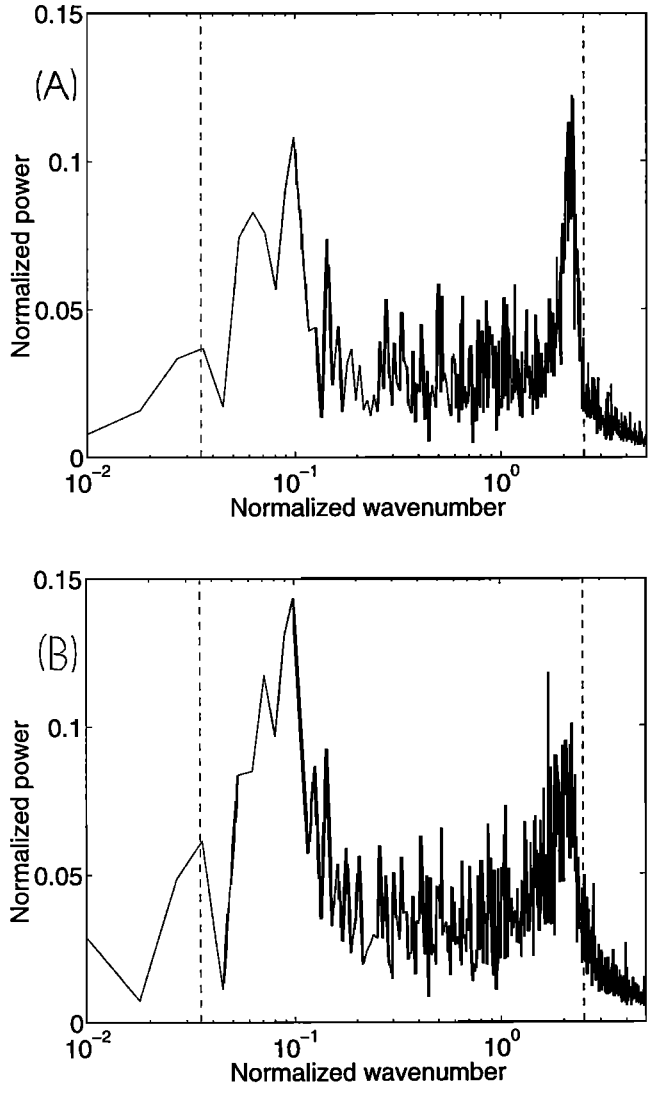

Figure 6. The normalized power of the wave modes as a function of $\tilde{k}$ for a weak emission and for $\omega_p/\omega_c > 1.7$. (a) The power in the first integration interval. (b) The power in the second integration interval. The power has been integrated over time. The dashed lines indicate the points where the solution of the linear dispersion relation crosses ω_{uh}.

to the wave in Figure 5 because the emission amplitude is one-fourth times that in section 4.1. The peak power of this wave is one-tenth times the peak power it has for the emission amplitude of 1.2 V/m and is thus higher than expected if we would assume the wave to be linear. Then the ratio should be 1/16. The self- interaction of the wave generated by the emission amplitude of 1.2 V/m transfers wave energy to its harmonics, some of which have values of $\tilde{\omega}, \tilde{k}$ corresponding to transiently damped waves. This energy is then absorbed.

We also notice the presence of a signal at $\tilde{k} \approx 2$, which is less than that of the intersection point at high $\tilde{k}$. This signal is not significantly stronger than that at $\tilde{k} = 0.035$ as we would expect from the antenna power distribution $P(k)$ in (4). This indicates that the peak in power at $\tilde{k} \approx 2$ is still nonlinearly damped.

The $\tilde{k}$ spectrum of the interval between $t = 60$ and $t = 80$ is shown in Figure 6b. If the wave peak at $\tilde{k} = 2$ was damped, one may expect a further reduction in the power for the second interval. This is confirmed by Figure 6b. Plotted is the normalized wave power versus $\tilde{k}$. The peak value at high $\tilde{k}$ has been reduced from 0.13 to 0.09.

In Figures 5, 6a, and 6b the wave packet at low $\tilde{k}$ has its maximum power at a higher $\tilde{k}$ than the intersection point between the undamped solution of the ECH wave mode and $\tilde{\omega}_0$. Since the upward shift is approximately the same in Figures 5, 6a, and 6b, it is likely to be a linear effect. From (2) we have the normalized frequency spread of the sounder pulse $\Delta\tilde{\omega} = (2\pi/\tau)/\omega_c$. For $\tau = 40 \times 2\pi/\omega_0$ and $\tilde{\omega}_0 = 2.1$ we get $\Delta\tilde{\omega} = 2.1/40 = 0.0525$. If $\tilde{\omega}_{\max}$ is the frequency of the (linear) ECH wave at $\tilde{k} \approx 0.08$ (the low $\tilde{k}$ peak), then $\tilde{\omega}_{\max} - \tilde{\omega}_{uh} \approx 0.0282$, which is less than $\Delta\tilde{\omega}$. The reason for the shifted power maximum may then be that the antenna couples more easily to waves with a high $\tilde{k}$.

The wave packet at $\tilde{\omega} \approx \tilde{\omega}_{uh}$ and at large $\tilde{k}$ is shifted toward lower $\tilde{k}$ than the intersection point of the linear dispersion relation with $\tilde{\omega}_{uh}$. The wave power peaks at $\tilde{k} \approx 2.23$ compared to $\tilde{k} = 2.5$ of the intersection point. The peak wave power is then shifted to $\tilde{\omega}_{\max} = 2.1277$. Here the difference $\tilde{\omega}_{\max} - \tilde{\omega}_{uh} = 0.0277$ is also less than $\Delta\tilde{\omega} = 0.0525$ of the emission. Here the shift might be a nonlinear effect. Decreasing $\tilde{k}$ and increasing $\tilde{\omega}_{\max}$ increases the estimate of E_{crit} in (1). The shift thus increases the maximum allowed wave power. A more detailed investigation of this shift is left to future work.

To show that the trapping of electrons by the ECH wave at $\tilde{k} \approx 2$ might be the damping mechanism, we compare the wave amplitudes of this wave packet with $E_{\text{crit}} = 0.03$ V/m (1). To obtain the wave amplitude of the wave packet centered at $\tilde{k} \approx 2$, we filter the electrostatic field distribution in the simulation box in $\tilde{k}$ at the time $t = 45$. The filter sets the amplitude spectrum for waves with $\tilde{k}$ other than $\tilde{k} \epsilon [1.7, 2.7]$ to zero. The result is shown in Figure 7. Plotted is the electric field amplitude of the wave packet centered at $\tilde{k} \approx 2$ as a function of the grid cell number. The modulus of the wave electric field exceeds $|E_{\text{crit}}|$ (the horizontal lines). The wave may thus trap electrons. Filtering the data set for the simulation with the emission amplitude 1.2 V/m reveals that at $t = 45$ no signal is present in the interval $\tilde{k} \epsilon [1.7, 2.7]$.

The peak at the low $\tilde{k}$ intersection point has increased its power. The overall change in power is, however, not large enough compared to noise levels to identify the reason for this since the peak covers only a small interval in $\tilde{k}$.

4.3. The Measurement of v_{th}

In section 2 the dependence of v_{gr} of the UH wave on v_{th} at low $\tilde{k}$ has been investigated. In this section

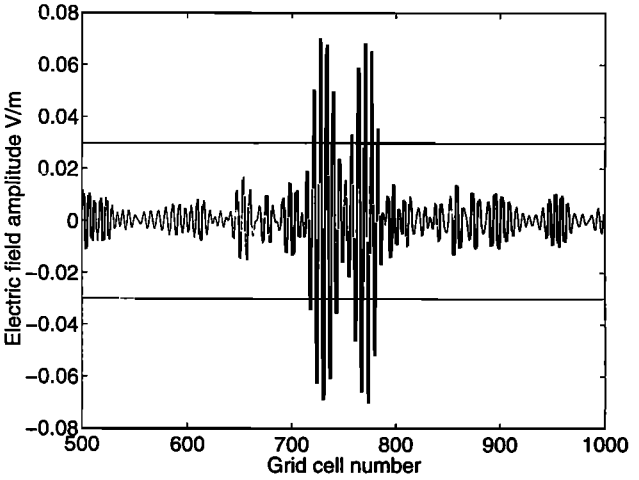

Figure 7. The electric field amplitude of the wave corresponding to the signal at $\tilde{k} \approx 2$ in Figures 6a and 6b for the time t=45. Overplotted as horizontal lines are $\pm E_{\text{crit}}$.

the numerical simulations revealed that emissions with a strong electric field amplitude cannot generate the linear wave at high $\tilde{k}$. The antenna length for the plasma sounder is known. The wave response duration can be measured. If the response is due to accompanying waves (that remain in the antenna's vicinity), one may be tempted to relate the antenna length divided by the response duration to the v_{gr} of the wave at low $\tilde{k}$. Then v_{gr} at $\tilde{\omega} \approx \tilde{\omega}_{uh}$ would determine v_{th}.

What is not known is to what extent we can apply the concept of the group velocity calculated for undamped linear ECH waves. Figure 5 showed that the wave packet is not centered at the intersection point of $\tilde{\omega} = \tilde{\omega}_{uh}$ and the undamped linear dispersion relation solution for the corresponding ECH wave branch. The group velocity for $\tilde{k} \approx 0.035$ (the intersection point) exceeds that at $\tilde{k} \approx 0.08$ (the signal's power peak) by less than 15%. The group velocity at $\tilde{k} \approx 0.08$ exceeds the minimum group velocity close to $\tilde{\omega}_{uh}$ by less than 5%. These velocity differences are probably negligible compared to modifications arising from uncertainties in the satellite motion or non-Maxwellian features in the electron distribution function (modifying the group velocity).

In addition, the absorption of wave energy by the trapped electrons and by wave-wave coupling may heat the plasma. This heating will increase the noise levels and may give rise to plasma instabilities which could affect the plasma response. For the considered simulation parameters the electron kinetic energy in the simulation box has increased by only 0.4%. If, like for the real sounder, electrons are also allowed to move along the magnetic field lines, an efficient relaxation mechanism for the electron distribution function is provided. For the considered plasma and emission parameters we may thus ignore heating.

The virtual antenna is now changed to an antenna with two plates on opposite potentials. Each plate is on $U_{\max} = 8.4$ V relative to the surrounding plasma. Between both antenna plates, $U_{\max}$ is thus 16.8 V. Both antenna plates are separated by 10 simulation grid cells, and the antenna length L is thus 70 m, which is comparable to that on board the Ulysses spacecraft.

The potential difference between the antenna plates is shown in Figure 8 as a function of the normalized time. The dashed vertical line indicates the end of the emission. Shortly after the emission starts, the potential difference is approximately that given by the forced oscillation. After a few emission periods the plasma response reduces the potential difference to a peak value of 10 V. After the emission has finished the peak potential difference drops to ≈ 2 V, which is still considerably higher than the noise levels for the simulation (≈ 0.1 V).

The antenna response spectrum is obtained by Fourier transforming the antenna's potential difference over time and squaring the result. This gives a power spectrum as a function of $\tilde{\omega}$. The window length is 40 time units. The integration interval starts first at $t = 40$, and the start is then shifted toward higher values of t. This gives an $\tilde{\omega}, t$ spectrogram. The two $\tilde{\omega}$- bins with the highest wave power are extracted and plotted as a function of $\hat{t} = t$ - 40, where t refers to the beginning of the integration interval. A time $\hat{t} = 0$ thus corresponds to an integration interval from $t = 40$ to $t = 80$. The power is normalized to the average power that would be present in the corresponding bin if no emission was present.

The $\tilde{\omega}$- bin with the most wave power over the longest time interval in the simulation is the one containing the frequency maximum of the ECH branch between points 1 and 2 in Figure 1. This maximum corresponds to a nonpropagating wave. Its normalized power as a function of $\hat{t}$ is plotted in Figure 9. This confirms that,

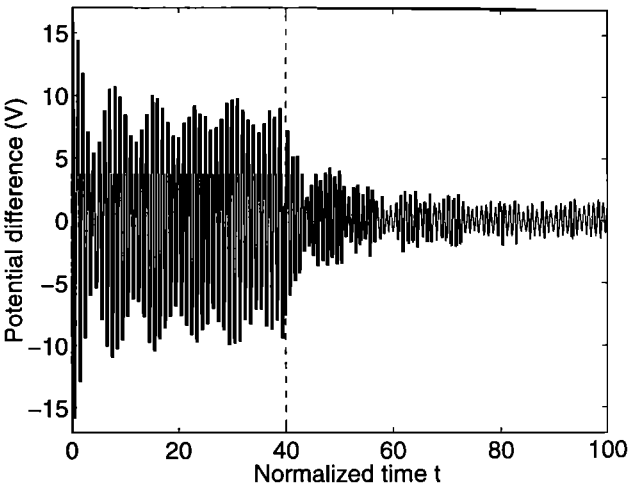

Figure 8. The potential difference between the antenna plates as a function of time. Plotted is the potential in volts as a function of the normalized time t for $\omega_p/\omega_c > 1.7$.

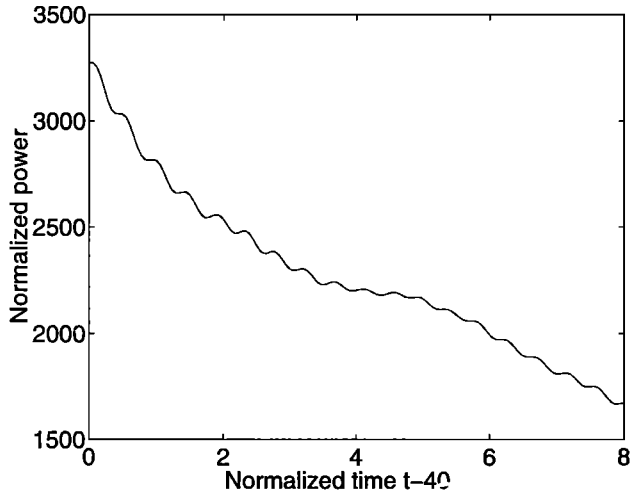

Figure 9. The power in the bin $\tilde{\omega} = 2.39$ as a function of the normalized time $\hat{t}$. The power is normalized to the noise power in this bin and $\omega_p/\omega_c > 1.7$.

at least for this simulation, the response maximum is given by an accompanying wave since the wave power stays close to the antenna. The power slowly drops because the (finite width) $\tilde{\omega}$- bin also contains propagating wave solutions. This resonance has been excited by the spread in $\tilde{\omega}$ of the emission, i.e. by the sidelobes of $P(\omega)$ in (2).

The second largest response is provided by the bin centered at $\tilde{\omega}_{uh}$. The power normalized to the noise power in this $\tilde{\omega}$- bin is plotted versus $\hat{t}$ in Figure 10. The power strongly drops until $\hat{t} \approx 2.7$, which is indicated by the dashed vertical line. Afterwards, the signal intensity starts to oscillate on a lower level than the initial intensity but still on a higher level than the noise background.

The physical parameters under consideration are $v_{th} \approx 9.4 \times 10^5$ m/s, $\omega_c = 10^4$ rad/s, and $\tilde{\omega}_{uh} = 2.1$. The minimum v_{gr} at $\tilde{\omega} \approx \tilde{\omega}_{uh}$ and at low $\tilde{k}$ ($\tilde{k} = 0.055$) is $v_{gr} \approx 5.4 \times 10^5$ m/s. Thus it should take the UH wave 2.7 wave periods to propagate over one antenna length of 70 m (thus leaving the interval between the antenna plates where it can be detected). This matches the time interval in Figure 10 up to which the signal intensity strongly decreased. The accompanying waves thus account for a substantial fraction of the plasma response. The power levels after $\hat{t} \approx 2.7$ are significantly higher than the noise levels without any emission.

This could be caused by wave components of the main signal reflected back to the antenna location by the noise fluctuations of the PIC code. The low numbers of particles per cell in a PIC simulation cause statistical fluctuations in the plasma density. These density fluctuations could then play a role equivalent to the density fluctuations in a "real" plasma which are held responsible for oblique echoes [*McAfee*, 1969].

A second possibility could be that the wave packet's end is not precisely defined. The wave packet encounters an unperturbed plasma in the direction it propagates. The wave amplitudes gradually increase. In the work of *Brillouin* [1960], it has been shown that the amplitude increase is accomplished by wave forerunners. These wave forerunners are typically transiently damped modes of the plasma. They do not necessarily have the group velocities calculated for the undamped plasma eigenmodes; that is, components of the wave packet can propagate considerably faster or slower than the main signal. This, together with the gradual increase of the electric field amplitude, complicates a strict definition of the wave packet's front. The end of the wave packet is equivalent to the switching on (after some time) of a second wave with the same frequency as the first wave but with a phase shifted by π. After some time the electric fields of the first and second waves cancel out to zero. The wave packet's end will thus consist of the transient wave modes of the second wave. It is thus equally complicated to define the end of a wave packet. One can therefore not expect the wave amplitudes to return immediately to noise levels after the main signal has left the space between the antenna plates. For a more profound discussion of wave forerunners, see the work of *Brillouin* [1960].

5. Simulated UH Emissions in a Strongly Magnetized Plasma

We now consider the case of only one nonpropagating wave at $\tilde{\omega}_{uh}$. Let $\omega_c = 11.5$ kHz ($\tilde{\omega}_{uh} = 1.9$) and $\tilde{\omega}_0 = \tilde{\omega}_{uh}$. Two simulations are performed. One applies

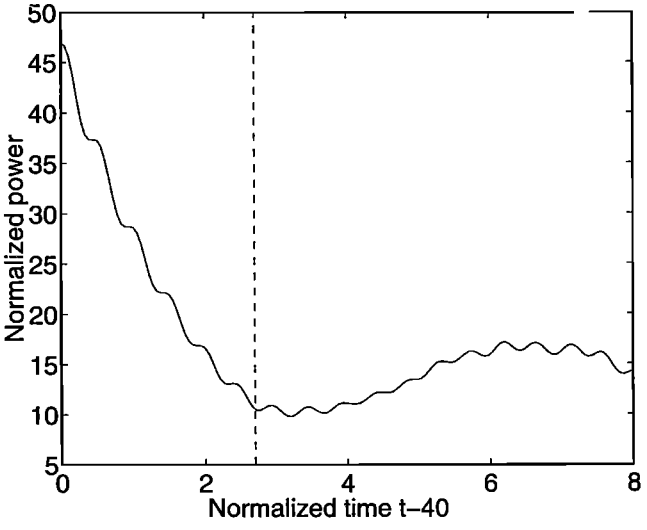

Figure 10. The power in the bin $\tilde{\omega} = 2.10$ as a function of the normalized time $\hat{t}$. The power is normalized to the noise power in this bin. The dashed line shows the time it takes the resonant wave to propagate over one antenna length and $\omega_p/\omega_c > 1.7$.

an electric field of 1.2 V/m to the antenna grid cells accounting for a potential difference between the antenna and the surrounding plasma of 8.4 V. The second simulation uses $1/\sqrt{2}$ times those values. We Fourier transform in space over the electric field data. We integrate the $\tilde{k}$- spectrum over the interval $\tilde{k} \in [0.02, 0.1]$. The normalized power is shown in Figure 11 as a function of t. The dashed line shows the power for the strong emission amplitude, and it is normalized to its peak value. The solid line shows the power for the weak emission amplitude, and it is normalized to half the peak value of the dashed line to account for the different emission amplitudes.

Both curves grow linearly at the same rate and reach the same power after the emission's end ($t = 40$). Then the power remains constant, indicating that no damping mechanism is present. Increasing the emission amplitude by a factor of $\sqrt{2}$ increases the wave power by a factor of 2. This shows that the emission is in a linear regime.

To understand how the energy is distributed in space, we Fourier transform over time. The integration time interval ranges from $t = 40$, i.e., $t = T$, up to $t = 106$. We examine the power in the two bins with the highest power, which are those at $\tilde{\omega} \approx 1.90$ and (the next lower bin) at $\tilde{\omega} \approx 1.87$. The distribution of the wave power as a function of the grid cell number for the strong emission amplitude and the weak emission amplitude in the bin at $\tilde{\omega} \approx 1.87$ is shown in Figure 12. The power is normalized to the peak power of the dashed line. The antenna is marked with vertical lines in Figures 12 and 13. Two wave packets propagate away from the antenna. This follows from the observation of a wave power minimum at the antenna's location. A second indicator is discussed below. As expected from Figure 11, the power for the dashed line is approximately twice as high as the power for the solid line. The generated wave packets are not symmetric with respect to the antenna's location. A possible reason for the asymmetry is the dispersive character of the excited wave modes. The energy of the wave packet is spread over a large

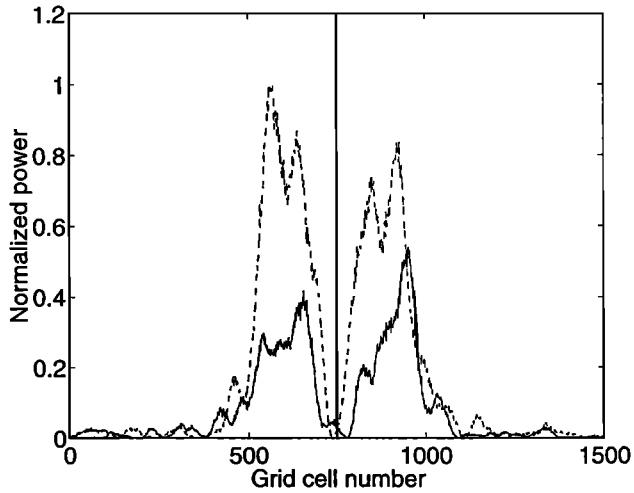

Figure 12. The wave power in the bin $\tilde{\omega} = 1.87$ as a function of the spatial grid cell number and for $\omega_p/\omega_c < 1.7$. The dashed line shows the power for the strong emission amplitude, and the solid line shows that for the weak emission amplitude. Both curves are normalized to the peak value of the dashed line.

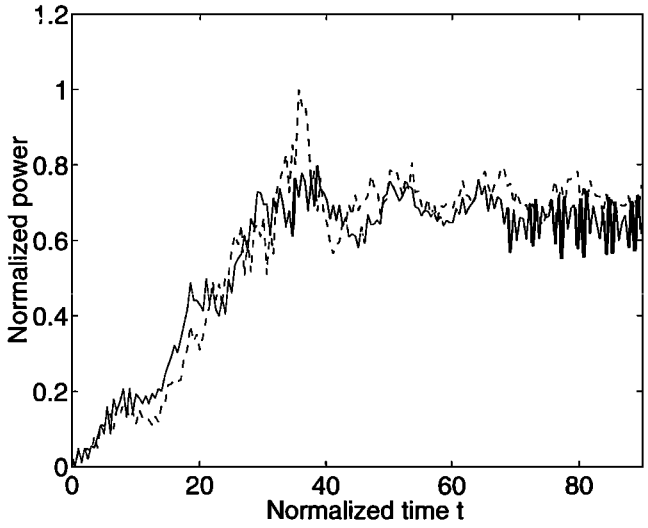

Figure 11. The power of the upper hybrid (UH) wave as a function of the normalized time t. The dashed line shows the power of the wave mode in the case of the strong emission and $\omega_p/\omega_c < 1.7$. It is normalized to its peak value. The solid line shows the curve for the weak emission amplitude. The curve is normalized to half the peak value of the dashed line.

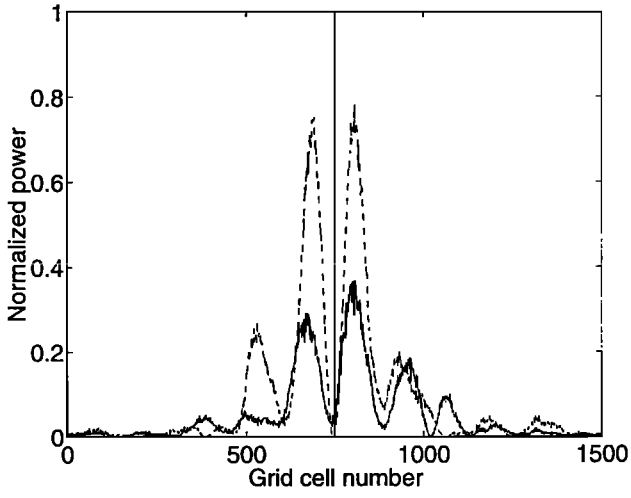

Figure 13. The wave power in the bin $\tilde{\omega} = 1.90$ as a function of the spatial grid cell number and for $\omega_p/\omega_c < 1.7$. The dashed line shows the power for the strong emission amplitude, and the solid line shows that for the weak emission amplitude. Both curves are normalized to the peak value of the dashed line in Figure 12.

interval in $\tilde{\omega}, \tilde{k}$. The wave packet's shape in space and time strongly depends on the phase and amplitude relations of the individual wave components. Simulation noise will modify these relations; thus the envelope in x, t of the wave packet will change.

The distribution for the bin at $\tilde{\omega} \approx 1.90$ is shown in Figure 13. The power is normalized to the peak power of the dashed line in Figure 12. The dashed line in Figure 13 shows the power distribution for the strong emission amplitude, and the solid line shows the one for the weak emission amplitude. The overall power for the dashed line is approximately twice the one for the solid line, but the power is distributed differently, possibly for the same reason as in Figure 12. The pronounced maxima and minima indicate a stationary standing wave because $v_{ph} \neq 0$ and because the extrema are fixed. The absence of pronounced power minima in Figure 12 is an indicator that the waves in Figure 12 propagate; that is, they are not standing waves.

The power of the standing wave decreases for increasing distances from the antenna, indicating that the waves are spatially damped. Since the plasma response has been shown to be linear, this damping should also be linear in which case the nonpropagating waves are weakly damped (transient) wave solutions of the linear dispersion relation.

Comparing Figures 12 and 13 suggests that a spacecraft moving at a velocity with respect to the plasma that is less than v_{gr} of the propagating waves in Figure 12 would not detect any response at $\tilde{\omega} \approx 1.87$. It may detect the power maxima in space at $\tilde{\omega} \approx 1.90$ (Figure 13) provided the waves are stable on a timescale that is long compared to the time it takes the satellite to reach the first power maximum.

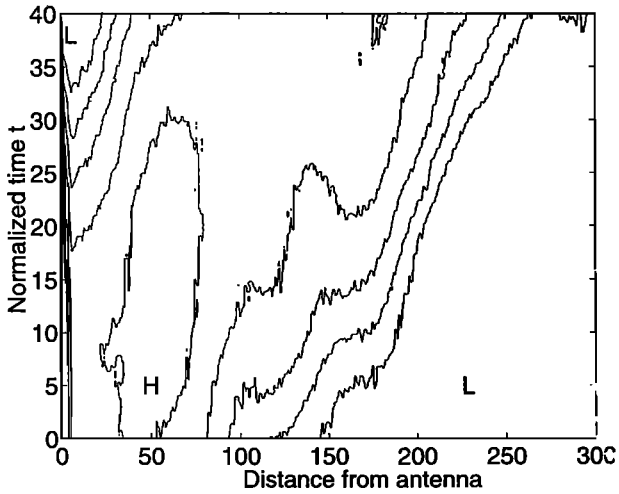

Figure 14. A contour plot of the spatial distribution of the wave power in the bin $\tilde{\omega} \approx 1.87$. The logarithmic power is plotted versus the grid cell number relative to the antenna and versus the normalized simulation time t. The contour lines are $10^{-4.1}$, $10^{-3.9}$, $10^{-3.7}$, $10^{-3.5}$, $10^{-3.25}$, and 10^{-3}.

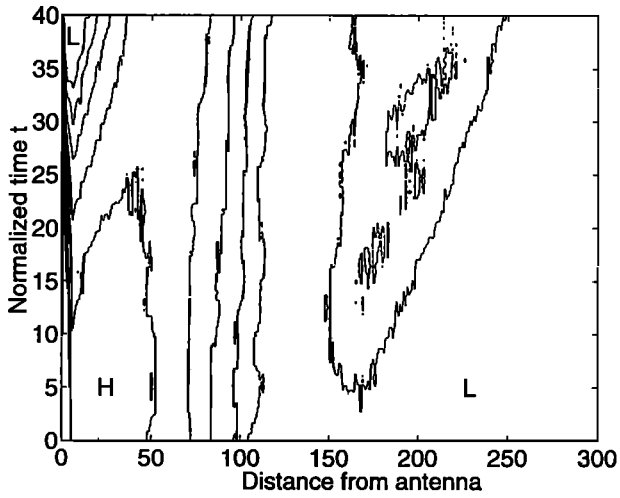

Figure 15. A contour plot of the spatial distribution of the wave power in the bin $\tilde{\omega} \approx 1.90$. The logarithmic power is plotted versus the grid cell number relative to the antenna and versus the normalized simulation time t. The contour lines are $10^{-4.1}$, $10^{-3.9}$, $10^{-3.7}$, $10^{-3.5}$, $10^{-3.25}$, and 10^{-3}.

The structures in Figures 12 and 13 have propagated to almost the same distance even though the range of v_{gr} of the waves in both $\tilde{\omega}$- bins differs. To identify a correlation between both structures, we plot the contour lines of the time-integrated power for both bins as a function of time. The full time integration window is over 66 emission wave periods. The interval starting point is shifted from $t = 0$ to $t = 40$. The same bins as for Figures 12 and 13 are taken. The power contained in the bin at $\tilde{\omega} \approx 1.87$ is shown in Figure 14. The power is normalized to the maximum power found in the bin at $\tilde{\omega} \approx 1.9$ at the antenna's location. The power is plotted versus the normalized time corresponding to the integration interval starting point and versus the distance in simulation grid cells from the sounder. The power of both wave packets propagating away from the antenna is averaged. The letter L indicates the regions with the lowest power whereas the H indicates the region with the highest power. The power increases from the regions denoted by L to the inside of the structures. One notices a structure propagating away from the antenna.

Figure 15 shows the signal in the bin at $\tilde{\omega} \approx 1.9$. Plotted is the power, normalized to the same value as that in Figure 14, versus the normalized time corresponding to the integration interval starting point and versus the distance in grid cells from the antenna. The contour lines are the same as those in Figure 14. The power maximum close to the antenna is strong and nonpropagating. It develops a minimum at the antenna's location at a normalized time of $t = 35$. The power distribution at time $t = 40$ is shown in Figure 13. Apart from the maximum at a distance of ≈ 50 grid cells, a second maximum builds up at a distance of 150 - 250 grid cells. The wave front of this maximum is strongly correlated

with that in Figure 14, which is in agreement with *Brillouin* [1960]. The emission with a finite time duration generates a wave packet with a frequency spread. The individual components propagate away from the antenna with their v_{gr}. At a spatial position different from the antenna position the wave components will arrive at different times. Since the wave front is associated with a signal growing in time, it will have a frequency spread. Thus the emission at $\tilde{\omega} \approx 1.9$ (a nonpropagating wave) generates a wave forerunner at a frequency $\tilde{\omega} \approx 1.87$ (a propagating wave). After having propagated a certain distance into the plasma, the forerunner couples back wave energy into the nonpropagating wave.

6. Discussion

The aim of this work has been to understand some fundamental properties of waves in a warm plasma close to ω_{uh}. This has been done with hindsight to the plasma sounding experiment since there ω_{uh} is an important resonance. Results known from linear kinetic theory have been applied to experimental observations. A quantitative explanation has been given for the absence of a plasma response at ω_{uh} in the hot parts of the magnetotail and in the Io plasma torus. It has been shown that the theory of accompanying waves can explain the change of the plasma response duration to sounding at ω_{uh} if the ratio ω_p/ω_c crosses a value of 1.7. This observation can also be explained by the theory of oblique echoes [*Benson*, 1982]. Explaining the change in the response duration by a change in v_{gr} can, however, also predict the order of magnitude of the response duration.

For $\omega_p/\omega_c < 1.7$ the UH waves do not propagate. If the plasma response in this case were due to accompanying waves, one would expect a long-lasting response to sounding. Then, however, it is not clear how the energy is transferred into the surrounding plasma. If we would relate the energy propagation velocity to the wave's v_{gr}, this would be impossible. Previously, the presence of wave forerunners has not been considered. The frequency spread of the emitted wave packet as well as the possible involvement of transiently damped wave modes in the emission process may allow an energy transfer with a nonzero velocity into the plasma by means of the forerunners. At the same time, the only waves at this frequency that are not spatially damped, the waves with $v_{gr} = 0$, do not propagate. The structure would then remain spatially confined.

We have shown that thermal effects alter the plasma resonance frequency close to ω_{uh} provided that the resonance is caused by accompanying waves. The resonance frequency shifts downward for a ratio of ω_p/ω_c of less than 1.7, and it shifts upward in the opposite case. Both modifications are, at least for the plasma parameters considered in this work, too small to seriously affect the interpretation of the sounder results.

As a next step, we investigated how the inclusion of both linear and nonlinear effects may affect the plasma response. For this purpose a set of one-dimensional electromagnetic PIC simulations have been performed.

For weakly magnetized plasmas we have shown that a strong emission leads to nonlinear damping up to the suppression of the linear wave at high $\tilde{k}$. As a likely candidate, electron trapping has been suggested here for two reasons. First, the values for E_{crit} estimated for the onset of trapping (equation (1)) have been exceeded by the electric field of the high $\tilde{k}$ wave. Second, the maximum electric fields also changed, as a function of $\tilde{k}$, qualitatively as expected for trapping (equation (1)); that is, the damping is more effective for the wave with a large $\tilde{k}$. For emission amplitudes that were lower than the ones for the real sounding experiment, the simulations showed that the UH wave at high $\tilde{k}$ could not be excited. This justified the focus on the UH wave at low $\tilde{k}$ in section 2.

A different damping mechanism, wave-wave coupling, affecting the wave at a low $\tilde{k}$, was less effective in suppressing this wave which is thus expected to provide, in most cases, the plasma response to sounding at ω_{uh}.

The PIC simulations have revealed the extent to which the v_{gr} given by the linear dispersion relation solution can be used to determine v_{th}. The attempt to relate the antenna length divided by the plasma response duration (which requires the plasma response to be due to accompanying waves) to v_{gr} has been proven successful. The case considered, i.e., a one-dimensional antenna at rest with respect to the plasma frame of reference, is, however, a very idealized case that may not be comparable to the real sounding experiment. By comparing the UH response durations given by the Alouette sounder with the response durations expected from linear theory, we have, however, shown that the response duration at ω_{uh} may indeed yield an estimate of v_{th}.

Sounding at ω_{uh} in a strongly magnetized plasma has been shown to create a nonpropagating standing wave. We have suggested that the buildup of the structure is achieved by forerunners. As a consequence, the energy remains confined since the only undamped wave solution at this frequency does not propagate. Emissions with two different electric field amplitudes showed that for the plasma and wave parameters considered the power transferred to the plasma increases quadratically with the emission amplitude and linearly with the time. This indicates that the plasma response in this case is linear.

The simulation results showed, for both magnetizations, that accompanying waves can account for a plasma response to sounding at ω_{uh}. The dependence $v_{gr}(\omega)$ for waves with $\omega \approx \omega_{uh}$ furthermore suggests that the frequency spread of the peak also depends on the magnetization. While the peak should have a narrow frequency band in strongly magnetized plasmas, it should have a wide frequency band in weakly magnetized plasmas. This is true provided the plasmas are sufficiently hot. For the cold plasmas found in the

ionosphere the minimum in v_{gr} close to ω_{uh} would get pronounced for $\omega_p/\omega_c > 1.7$, and thus the UH response peak would be sharp.

Acknowledgments. Mark Dieckmann has been partially supported throughout this work by a Warwick fellowship and by the CNRS Orléans. The work has been finished under support of the European network grant FMRX-CT98-0168 and of a University of Linkoeping fellowship. Sandra C. Chapman was supported by PPARC. The authors would like to thank the NSC in Linkoeping, Sweden, for the generous provision of computer time on its Cray T3E. The authors would also like to thank V. V. Krasnosel'skikh and P. M. E. Décréau for the discussions contributing to this work

Hiroshi Matsumoto thanks T. Ono and another referee for their assistance in evaluating this paper.

References

Akhiezer, A. I., I. A. Akhiezer, R. V. Polovin, A. G. Sitenko, and K. N. Stepanov, *Plasma Electrodynamics,* vol. 1, *Linear Theory,* 237 pp., Pergamon, Tarrytown, N. Y., 1975.

Baumjohann, W., and R. A. Treumann, *Basic Space Plasma Physics,* 7 pp., Imperial Coll. Press, London, 1997.

Benson, R. F., Stimulated plasma waves in the ionosphere, *Radio Sci., 12,* 861-878, 1977.

Benson, R. F., Stimulated plasma instability and nonlinear phenomena in the ionosphere, *Radio Sci., 17,* 1637-1659, 1982.

Benson, R. F., J. Fainberg, R. A. Hess, V. A. Osherovich, and R. G. Stone, An explanation for the absence of sounder-stimulated gyroharmonic resonances in the Io plasma torus by the Ulysses relaxation sounder, *Radio Sci., 32,* 1127-1134, 1997.

Brillouin, L., *Wave Propagation and Group Velocity,* Academic, San Diego, Calif., 1960.

Décréau, P. M. E. et al., 'Whisper': A sounder and high-frequency wave analyser experiment, *Eur. Space Agency Spec. Publ., ESA SP-1159,* 49-68, 1993.

Dieckmann, M. E., S. C. Chapman, A. Ynnerman, and G. Rowlands, The energy injection into waves with a zero group velocity, *Phys. Plasmas, 6,* 2681-2692, 1999.

Etcheto, J., H. de Feraudy, and J. G. Trotignon, Plasma resonance stimulation in space plasmas, *Adv. Space Res., 1,* 183-196, 1981.

Fejer, J. A., and W. Calvert, Resonance effects of electrostatic oscillations in the ionosphere, *J. Geophys. Res., 69,* 5049-5062, 1964.

Krall, N. A., and A. W. Trivelpiece, *Principles of Plasma Physics,* 405 pp., San Francisco Press, San Francisco, Calif., 1986.

Le Sager, P., P. Canu, and N. Cornilleau-Wehrlin, Impact of the Ulysses velocity on the diagnosis of the electron density by the Unified Radio and Plasma Wave sounder in the outskirts of the Io torus, *J. Geophys. Res., 103,* 26,667-26,677, 1998.

McAfee, J. R., Topside ray trajectories in an anisotropic plasma near plasma resonances, *J. Geophys. Res., 74,* 6403-6408, 1969.

Meyer-Vernet, N., S. Hoang, and M. Moncuquet, Bernstein waves in the Io plasma torus: A novel kind of electron temperature sensor, *J. Geophys. Res., 98,* 21,163-21,176, 1993.

Riyopoulos, S., Nonlinear Landau damping of purely perpendicular Bernstein modes, *J. Plasma Phys., 36,* 111-125, 1986.

Roennmark, K., and P. J. Christiansen, Dayside electron cyclotron harmonic emissions, *Nature, 294,* 335-338, 1981.

Warren, E. S., and E. L. Hagg, Observation of electrostatic resonances of the ionospheric plasma, *Nature, 220,* 466-468, 1968.

S. C. Chapman and G. Rowlands, Space and Astrophysics Group, Physics Department, University of Warwick, Coventry CV 47 AL, England, U. K. (sandrac@astro.warwick.ac.uk; g.rowlands@warwick.ac.uk)

M. E. Dieckmann and A. Ynnerman, ITN, University of Linkoeping, Campus Norrkoeping, 60174 Norrkoeping, Sweden. (mardi@itn.liu.se; andyn@itn.liu.se)

(Received December 18, 1998; revised November 25, 1999; accepted November 25, 1999.)